Alternative Mechanism for $\omega_0/2$ Emission in Laser-Produced Plasmas

K. L. Baker, K. G. Estabrook, R. P. Drake,* and B. B. Afeyan†

University of California–Davis and Lawrence Livermore National Laboratory, Livermore, California 94551

(Received 12 May 2000)

Several models have been proposed to explain the broad spectral features characteristic of $\omega_0/2$ emission observed in laser-produced plasmas. In this article, the electromagnetic decay instability is examined as an alternative explanation for this emission. It is shown that the electromagnetic decay instability is able to explain some of the spectral features observed from laser-produced plasmas. In addition, the electromagnetic decay instability is consistent with two other features observed in experiments: the efficient generation of electromagnetic energy and the discrepancy in the levels of emission between the $\omega_0/2$ emission and the $3\omega_0/2$ emission.

DOI: 10.1103/PhysRevLett.86.3787 PACS numbers: 52.35.Mw, 52.25.Os, 52.38.Dx, 52.38.-r

Many experiments have measured electromagnetic emission in laser-produced plasmas near half the laser frequency [1–3]. This electromagnetic emission, known as $\omega_0/2$ emission, has been attributed to Langmuir waves driven by the two-plasmon decay instability near the quarter-critical surface. A representative spectrum of $\omega_0/2$ emission is shown in Fig. 1. This spectrum originated from a carbon-hydrogen spherical target illuminated with 351 nm light at an average intensity of approximately 8×10^{14} W/cm^2 [1]. The estimated electron temperature, T_e, and density scale length, L_n, were 1 keV and 20 to 50 μm, respectively [1]. The spectrum shows two broad peaks, $\Delta\omega/\omega = 0.02$ [1,2], which are redshifted [1(c)] and blueshifted [1(b)] from half the laser frequency. Figure 1 also shows one narrow peak, $\Delta\omega/\omega = 0.004$ [1,2], which is redshifted [1(a)] by approximately half the amount of the broad red peak [1(c)]. The lower intensity at which the narrow feature [1(a)] was observed relative to the broad features [1(b) and 1(c)] allowed the authors in [1,2] to attribute the narrow feature [1(a)] to the high frequency mixed polarization instability, whose theory has been developed by Afeyan [4,5].

Quantitative measurements of the magnitude of the scattered $\omega_0/2$ emission have been taken with respect to $3\omega_0/2$ emission observed in the same experiments, as shown in Fig. 2. The $3\omega_0/2$ emission has been attributed to Thomson upscattering of the incident pump beam from Langmuir waves at the quarter-critical surface. As shown in Fig. 2, the $\omega_0/2$ feature, which is damped more heavily than the $3\omega_0/2$ feature, can contain nearly 4 orders of magnitude more energy than the $3\omega_0/2$ feature.

Previous experiments have also measured the energy contained in the Langmuir waves driven by two-plasmon decay. These experiments found a close correlation between the relative levels of x-ray emission from hot electrons and scattered $3\omega_0/2$ emission, allowing them to conclude that the electrons resulted from two-plasmon decay. These experiments have inferred from the measured x-ray emission that approximately 10^{-4} of the incident laser energy is contained in hot electrons attributed to two-plasmon decay [6,7]. In similar experiments, 5×10^{-6} of the laser energy was found in $\omega_0/2$ emission [1]. When the damping of the $\omega_0/2$ emission as it leaves the plasma is accounted for, the energy contained in the $\omega_0/2$ light can represent as much as 20% of the energy observed in hot electrons. This number then represents an upper limit on the conversion efficiency of the Langmuir wave energy into electromagnetic emission.

Several models have been proposed in the literature to explain the broad spectral features characteristic of $\omega_0/2$ emission observed in laser-produced plasmas [1,2,8–11]. Any mechanism proposed to explain the electromagnetic emission near $\omega_0/2$ seen in experiments must reproduce the spectral features of this emission and allow for a large disparity in the energy between the $\omega_0/2$ emission and the $3\omega_0/2$ emission. In addition, any mechanism which attributes the $\omega_0/2$ emission solely to the Langmuir waves produced near the quarter-critical surface must allow for

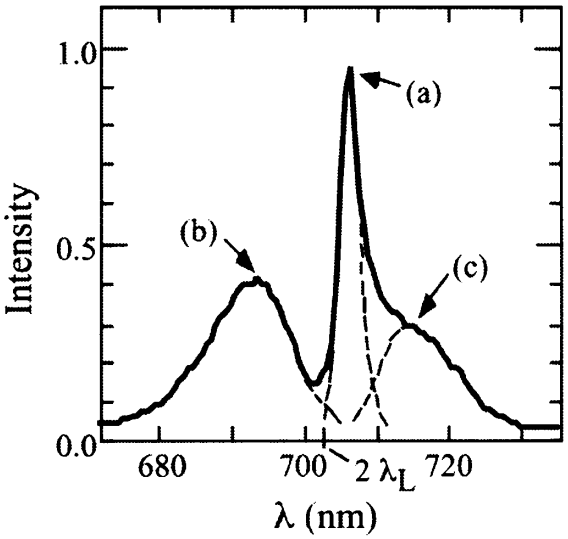

FIG. 1. Plot of the $\omega_0/2$ emission observed from a solid target experiment. The vertical axis shows the relative emission while the horizontal axis shows the wavelength of the scattered light. (Reprinted with permission from Seka *et al.* [1].)

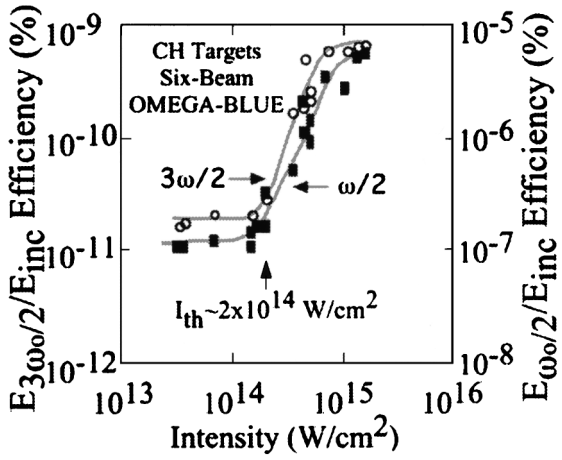

FIG. 2. Plot of the absolute magnitude of $3\omega_0/2$ emission and $\omega_0/2$ emission as a function of incident laser intensity. The left vertical axis shows the absolute $3\omega_0/2$ emission and the right vertical axis shows the absolute $\omega_0/2$ emission, while the horizontal axis shows the intensity of the incident laser. (Reprinted with permission from Seka *et al.* [1].)

an efficient conversion of the Langmuir wave energy into $\omega_0/2$ emission, as high as 20%.

Inverse-resonance absorption of Langmuir waves near the quarter-critical surface has been proposed as an explanation for the $\omega_0/2$ emission seen in experiments. The two-plasmon decay instability drives Langmuir waves that are redshifted and blueshifted from half the incident pump beam frequency. The blueshifted Langmuir waves travel up the density gradient; however, the redshifted Langmuir waves travel down the density gradient and cannot undergo inverse-resonance absorption unless the wave vectors are changed by auxiliary processes. In addition, most of the Langmuir wave's energy would be lost before it reached its critical surface due to Landau and collisional damping. The maximum conversion efficiency obtainable from the inverse-resonance absorption of Langmuir wave energy into electromagnetic emission is approximately 50% [12,13]. Langmuir waves whose perpendicular component of their wave number, with respect to the density gradient, is greater than half of the incident pump wave number cannot undergo inverse-resonance absorption because the required electromagnetic wave would not be a normal mode of the plasma. Because of these restrictions, the phase space of plasmons available for conversion into electromagnetic radiation is small. Inverse-resonance absorption therefore has a difficult time explaining the efficiencies observed in these experiments. Without significant perturbations to the background density to reduce the plasma scale length and allow for conversion of redshifted Langmuir waves, inverse-resonance absorption does not present itself as a likely candidate to explain the emission observed in experiments.

Thomson downscattering of the incident pump beam from Langmuir waves near the quarter-critical surface has also been proposed as an explanation for the features observed in experiments. To be a resonant Thomson scattering process, the interaction beam scatters from Langmuir waves which satisfy the wave number and frequency matching conditions for the Thomson scattering process, as well as the waves' respective dispersion relation. As a consequence, resonant Thomson downscattering cannot explain the $\omega_0/2$ spectrum for wavelengths greater than approximately 706 nm, the wavelength corresponding to the peak in Fig. 1(a). That implies that resonant Thomson scattering cannot explain the broad red peak shown in Fig. 1(c), as these would be evanescent waves. In addition, only the density range from $n_e/n_{cr} = 0.228$ to $n_e/n_{cr} = 0.246$ can contribute to the frequency spectrum represented by the broad blue peak in Fig. 1(b). Therefore, only about a third of the potential density range can contribute to the spectrum observed in the broad blue peak [1(b)]. In the density range $n_e/n_{cr} = 0.228$ to $n_e/n_{cr} = 0.246$, the Langmuir wave vectors of the primary two-plasmon decay instability do not have the appropriate wave vector to participate directly in a resonant Thomson scattering process. The wave vectors of these primary Langmuir waves must be changed both in magnitude and angle by processes such as the Langmuir decay instability or changes to the background density profile, so that they possess the appropriate wave vector to participate in resonant Thomson downscattering. Only a very small fraction of these Langmuir waves would then have the appropriate wave vector to be resonant. This small fraction would not be able to explain the efficiencies observed in the experiment. Even with these processes, resonant Thomson downscattering cannot explain the broad red peak shown in Fig. 1(c).

The electromagnetic decay instability (EDI) involves the decay of a Langmuir wave into an electromagnetic wave and an ion acoustic wave. Because the ion acoustic wave is a low frequency wave, the frequency of the electromagnetic daughter wave is very close to the frequency of the pump Langmuir wave. This has led to the use of EDI as an explanation for electromagnetic emission near the plasma frequency observed in laboratory-electron-beam instability experiments [14], type III solar bursts [15,16], and recently in ionospheric heating experiments [17]. The simultaneous evolution of EDI with the decay of the Langmuir wave into another Langmuir wave and an ion acoustic wave has also been studied [18].

To be resonant, EDI must satisfy frequency and wave vector matching conditions expressed as $\omega_{Lw} = \omega_s + \omega_{ia}$ and $\vec{k}_{Lw} = \vec{k}_s + \vec{k}_{ia}$, respectively. In these expressions, $\omega_{Lw}, \vec{k}_{Lw}; \omega_s, \vec{k}_s; \omega_{ia}, \vec{k}_{ia}$ are the frequency and wave vector for the Langmuir wave, the electromagnetic wave, and the ion acoustic wave, respectively. The frequency matching condition, in conjunction with the dispersion relations of the participating waves, imply that the wave number of the electromagnetic wave is $|k_s| \approx \sqrt{3}\,(v_{th}/c)\,|k_{Lw}|$, where v_{th} is the electron thermal velocity, and c is the speed of light. Because $|k_s| \ll |k_{Lw}|$,

the wave vector matching conditions further imply that $\vec{k}_{\rm ia} \approx \vec{k}_{\rm Lw}$. Therefore, a large number of decay triangles can resonantly interact with a single ion wave vector driving it up to a high level.

To explain the $\omega_0/2$ emission shown in Fig. 1, the electromagnetic decay instability must reproduce the spectral characteristics. The frequency shifts of the two Langmuir waves associated with two-plasmon decay can be calculated from their respective dispersion relation along with the two-plasmon decay frequency and wave number matching conditions [3]. In the reference frame moving at the velocity of the quarter-critical surface, the plasma waves are upshifted and downshifted from half of the "observed" laser frequency, $\omega_{\rm ob}$, by $\Delta\omega = \pm[(3\sqrt{3})/2](v_{\rm th}^2/c)\{(\vec{k}_{\rm Lwb}\cdot\vec{k}_0)/k_0 - \frac{1}{2}k_0\}$ [3], where $\vec{k}_{\rm Lwb}$ is the wave vector of the blue plasmon, and $\vec{k}_0$ is the wave vector of the incident electromagnetic wave. In this reference frame, the electromagnetic waves, ω_α, are redshifted from the frequencies corresponding to the Langmuir waves by their respective ion acoustic shifts or $\omega_\alpha = \omega_{\rm ob}/2 \pm \Delta\omega - c_s k_\alpha$.

Calculation of the observed laser frequency, $\omega_{\rm ob}$, in the plasma frame and the measured electromagnetic wave spectrum, $\omega_{\rm sblue}$ and $\omega_{\rm sred}$ in the laboratory frame must include frequency shifts of the electromagnetic waves due to the flowing plasma [19,20]. One contribution is from the Doppler shift arising from the relative motion of the quarter-critical surface and the laboratory frame, $\Delta\omega_{\rm D}/\omega = u_f/c$, where ω is the frequency of the electromagnetic wave, and u_f is the flow velocity of the plasma. The second contribution is from the time dependent changes in the plasma medium through which the electromagnetic wave is traveling, $\Delta\omega_{0P} = (\frac{1}{2}c)\int(\partial\omega_{pe}^2/\partial t)\,dx/(\omega^2 - \omega_{pe}^2)^{0.5}$ [19,20], where ω_{pe} is the electron plasma frequency. In this article, an isothermal rarefaction, $n(x,t) = n_{\rm cr}\exp[-(x - x_c)/c_s t]$, is assumed for the density profile with the plasma flow antiparallel to the incident pump wave number. In the moving plasma frame, the laser frequency observed by the plasma waves, $\omega_{\rm ob}$, is shifted due to both the time dependent changes in the plasma medium, $\Delta\omega_{0P}/\omega_0 \sim (0.31)(c_s/c)$, and the Doppler shift arising from the expanding quarter-critical surface, $\Delta\omega_{\rm D}/\omega_0 \sim (u_f/c)$, or $\omega_{\rm ob} = \omega_0(1 + 0.31c_s/c + u_f/c)$ [20]. In the laboratory frame where the electromagnetic waves resulting from EDI are recorded, the electromagnetic waves are shifted by both a Doppler shift, $\Delta\omega_{\rm D}/\omega_0 \sim 0.5(u_f/c)$, and a shift due to the time dependent changes in the plasma medium, $\Delta\omega_{0P}/\omega_0 \sim (0.31)(c_s/c)$, such that $\omega_{\rm sblue}$ and $\omega_{\rm sred} = \omega_\alpha + 0.5\omega_0(u_f/c) + 0.31\omega_0(c_s/c)$. The frequencies observed in the laboratory frame are then

$$\omega_{\rm sblue} = \frac{\omega_0}{2} + \frac{3\sqrt{3}}{2}\frac{v_{\rm th}^2}{c}\left(\frac{\vec{k}_{\rm Lwb}\cdot\vec{k}_0}{k_0} - \frac{1}{2}k_0\right) - c_s k_{\rm Lwb} + 0.46\omega_0\frac{c_s}{c} + \omega_0\frac{u_f}{c} \quad (1)$$

and

$$\omega_{\rm sred} = \frac{\omega_0}{2} - \frac{3\sqrt{3}}{2}\frac{v_{\rm th}^2}{c}\left(\frac{\vec{k}_{\rm Lwb}\cdot\vec{k}_0}{k_0} - \frac{1}{2}k_0\right) - c_s k_{\rm Lwr} + 0.46\omega_0\frac{c_s}{c} + \omega_0\frac{u_f}{c}, \quad (2)$$

where $\omega_{\rm sblue}$ and $\omega_{\rm sred}$ are the scattered light frequencies in the laboratory frame resulting from the blue and red plasmon, respectively.

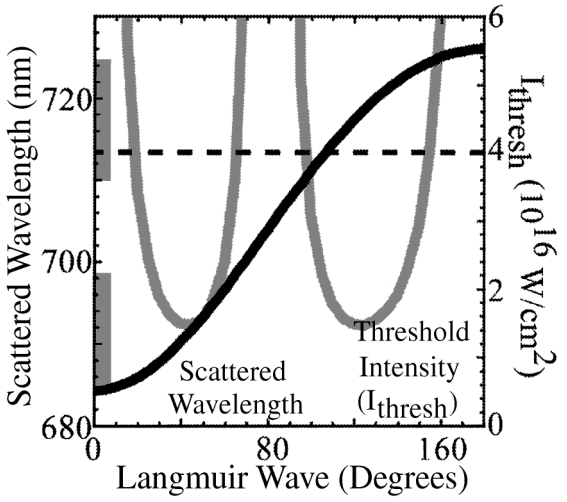

FIG. 3. Plot of the scattered frequency of the EDI generated electromagnetic wave, solid black line, as a function of Langmuir wave angle. This figure assumes an electron temperature of 1 keV, an incident laser wavelength of 351 nm, an effective ionization state of $Z = 3.5$, a flow velocity equal to twice the sound speed, and an electron density normalized to the incident lasers' critical density of $n_e/n_{\rm cr} = 0.2$. These parameters were chosen to match those present in Figs. 1 and 2. The solid gray lines represent the threshold intensity for the original two-plasmon decay instability. The gray bars represent the regions over which the two-plasmon decay instability is below threshold assuming the pump intensity is 4×10^{16} W/cm^2, denoted by the dashed black line.

Figure 3 shows the wavelength spectrum calculated using Eqs. (1) and (2). The solid black line represents the frequency of the scattered electromagnetic wave resulting from the decay of the Langmuir waves driven by two-plasmon decay. This frequency is plotted as a function of the Langmuir wave angle. The two solid gray curves in Fig. 3 denote the threshold laser intensity for the absolutely unstable two-plasmon decay instability in the presence of collisional and Landau damping [5]. This threshold is also plotted as a function of the Langmuir wave angle. Figure 3 shows that the minimum threshold occurs for the decay geometry in which the red plasmon driven by two-plasmon decay is scattered at 125°(235°) while the blue plasmon is scattered at approximately 315°(45°) relative to the incident pump wave vector. When these plasmons participate in EDI, the decay geometry corresponds to scattered

electromagnetic waves at 719 and 692 nm, respectively, as denoted by the solid black line. An incident laser intensity of 4×10^{16} W/cm^2, denoted by the dashed horizontal black line, was chosen to match the spectrum shown in Fig. 1. At 4×10^{16} W/cm^2, all Langmuir waves between 100°–155°(207°–262°) and 297°–342°(20°–65°) relative to the incident pump wave vector are driven absolutely unstable. The two gray bars located on the left side of Fig. 3 represent the portion of the EDI spectrum that is driven by the above-threshold two-plasmon decay plasmons. The wavelength range covered by these two gray bars matches very closely the spectral width observed in the experiment [1] shown in Fig. 1. Additional secondary decay processes, such as the Langmuir decay instability, would likely broaden the Langmuir wave spectrum beyond the primary Langmuir wave spectrum used to calculate the spectral width in Fig. 3.

The maximum conversion efficiency of Langmuir wave energy into electromagnetic wave energy was approximately 20%, based on measurements of $\omega_0/2$ emission [1,2] and energy attributed to hot electrons [6,7]. The measurement of hot electrons included contributions from the primary Langmuir wave spectrum, as well as secondary Langmuir waves driven by the Langmuir decay instability, which are also subject to decay via the EDI. This shows that there is enough energy in the Langmuir waves to explain the levels of $\omega_0/2$ emission observed in experiments. These conversion efficiencies are similar to efficiencies measured in laboratory-electron-beam instability experiments [14,21]. In this beam plasma experiment, electromagnetic emission near the plasma frequency was observed in conjunction with ion acoustic waves that had wave numbers approximately equal to the beam excited electron plasma waves, as expected in EDI. This experiment measured power conversion efficiencies of less than 17% [14,21], similar to the efficiencies inferred in the laser-plasma experiments. In addition, all of the Langmuir waves driven by the two-plasmon decay instability, as well as secondary instabilities, can undergo conversion into electromagnetic waves via the electromagnetic decay instability. EDI does not require propagation of or changes in the wave vectors of the Langmuir waves as the inverse-resonance absorption and Thomson scattering models require.

The energy disparity between the $\omega_0/2$ emission and the $3\omega_0/2$ emission observed in the experiment [1,2] can be explained by attributing the two features to different mechanisms. As shown above, the level of $\omega_0/2$ emission observed in the experiment is consistent with the levels expected from the electromagnetic decay instability given the measured energy in the Langmuir waves [6,7] and previous observations of EDI efficiencies [14,21]. The $3\omega_0/2$ emission levels observed in the experiments can then be attributed to Thomson upscattering of the pump electromagnetic wave from the Langmuir waves driven by the primary two-plasmon decay instability [1,2], as well as secondary processes such as the Langmuir decay instability and related strong turbulence processes [22,23].

The authors acknowledge useful discussions with T. W. Johnston, D. E. Hinkel, M. V. Goldman, W. Seka, D. F. DuBois, and H. Rose.

*Present address: University of Michigan, Ann Arbor, Michigan 48109-2143.
†Present address: Polymath Associates, Pleasanton, California 94566.

[1] W. Seka *et al.,* Phys. Fluids **28**, 2570 (1985).
[2] L. M. Goldman *et al.,* Can. J. Phys. **64**, 969 (1986).
[3] R. L. Berger and L. V. Powers, Phys. Fluids **28**, 2895 (1985).
[4] B. B. Afeyan and E. A. Williams, Phys. Rev. Lett. **75**, 4218 (1995).
[5] B. B. Afeyan and E. A. Williams, Phys. Plasmas **4**, 3845 (1997).
[6] M. C. Richardson *et al.,* Phys. Rev. Lett. **54**, 1656 (1985).
[7] D. M. Villeneuve *et al.,* Phys. Fluids **27**, 721 (1984).
[8] R. L. Berger (private communication).
[9] K. L. Baker, Ph.D. thesis, University of California–Davis, 1996.
[10] K. L. Baker *et al.,* in *Proceedings of the 24th Annual Anomalous Absorption Conference, Asilomar, Monterey, California, 1994* (Lawrence Livermore National Laboratory, Livermore, CA, 1994).
[11] D. Russel, D. F. DuBois, and H. Rose, in *Proceedings of the 24th Annual Anomalous Absorption Conference, Asilomar, Monterey, California, 1994* (Ref. [10]).
[12] D. E. Hinkel-Lipsker, B. D. Fried, and G. J. Morales, Phys. Rev. Lett. **62**, 2680 (1989).
[13] W. L. Kruer, *The Physics of Laser Plasma Interactions* (Addison-Wesley, Redwood City, CA, 1988).
[14] P. K. Shukla *et al.,* Phys. Rev. A **27**, 552 (1983).
[15] R. P. Lin *et al.,* Astrophys. J. **308**, 954 (1986).
[16] D. B. Melrose and M. V. Goldman, Sol. Phys. **107**, 329 (1987).
[17] T. B. Leyser, Phys. Plasmas **1**, 2003 (1994).
[18] S. L. Musher, A. M. Rubenchik, and V. E. Zakhorov, Phys. Rep. **252**, 178 (1995).
[19] E. F. Gabl *et al.,* Phys. Fluids B **1**, 1850 (1989).
[20] T. Dewandre, J. R. Albritton, and E. A. Williams, Phys. Fluids **24**, 528 (1981).
[21] D. A. Whelan and R. L. Stenzel, Phys. Rev. Lett. **47**, 95 (1981).
[22] D. F. Dubois, D. A. Russel, and Harvey A. Rose, Phys. Rev. Lett. **74**, 3983 (1995).
[23] J. Meyer and Y. Zhu, Phys. Rev. Lett. **71**, 2915 (1993).